Orthogonal Biofunctionalization of Magnetic Nanoparticles via "Clickable" Poly-(Ethylene Glycol) Silanes: A "Universal Ligand" Strategy to Design Stealth and Target-Specific Nanoca...

ARTICLE *in* JOURNAL OF MATERIALS CHEMISTRY · SEPTEMBER 2012

Impact Factor: 7.44 · DOI: 10.1039/C2JM34571D

6 AUTHORS, INCLUDING:

Debarati Bandyopadhyay
Indian Institute of Science
2 PUBLICATIONS **6** CITATIONS
SEE PROFILE

Harshad Harde
Intas Pharmaceuticals Ltd.
20 PUBLICATIONS **169** CITATIONS
SEE PROFILE

Sunil Kumar
Indus International University
13 PUBLICATIONS **71** CITATIONS
SEE PROFILE

Journal of
Materials Chemistry

Cite this: DOI: 10.1039/c2jm34571d

www.rsc.org/materials

PAPER

Orthogonal biofunctionalization of magnetic nanoparticles *via* "clickable" poly(ethylene glycol) silanes: a "universal ligand" strategy to design stealth and target-specific nanocarriers†

Manasmita Das,*[a] Debarati Bandyopadhyay,[b] Raman Preet Singh,[a] Harshad Harde,[a] Sunil Kumar[a] and Sanyog Jain*[a]

Received 12th July 2012, Accepted 24th September 2012
DOI: 10.1039/c2jm34571d

The present work demonstrates a novel strategy to synthesize orthogonally bio engineered magnetonanohybrids (MNPs) through the design of versatile, biocompatible linkers whose structure includes: (i) a robust anchor to bind with metal oxide surfaces; (ii) tailored surface groups to act as spacers and (iii) a general method to implement orthogonal functionalizations of the substrate *via* "click chemistry". Ligands that possess the synthetic generality of features (i) (iii) are categorized as "universal ligands". Herein, we report the synthesis of a novel, azido terminated poly(ethylene glycol) (PEG) silane that can easily self assemble on MNPs through hetero condensation between surface hydroxyl groups and the silane end of the ligand, and simultaneously provide multiple clickable sites for high density, chemoselective bio conjugation. To establish the universal ligand strategy, we clicked alkyl functionalized folate onto the surface of PEGylated MNPs. By further integrating a near infrared fluorescent (NIRF) marker (Alexa Fluor 647) with MNPs, we demonstrated their folate receptor mediated internalization inside cancer cells and subsequent translocation into lysosomes and mitochondria. *Ex vivo* NIRF imaging established that the azido PEG silane developed in course of the study can effectively reduce the sequestration of MNPs by macrophage organs (*viz.* liver and spleen). These folate PEG MNPs were not only stealth and noncytotoxic but their dual optical and magnetic properties aided in tracking their whereabouts through combined magnetic resonance and optical imaging. Together, these results provided a strong motivation for the future use of the "universal ligand" strategy towards development of "smart" nanohybrids for theragnostic applications.

1. Introduction

Polyethylene glycol (PEG) conjugation chemistry, also named as "PEGylation", is a very well known strategy for tailored modi fication of bio molecules including proteins, peptides, and enzymes, as well as drug delivery systems (DDS) based on lipo somes, dendrimers and inorganic organic hybrid nano particles.[1–4] Research in cell targeting and molecular imaging has extensively used functionalized PEG molecules as spacers between the concerned targeting/imaging modules and the ther apeutic vector.[5–10] In all these cases, PEGylation results in improved solubility and prolonged residence time in blood circulation, thereby avoiding degradation of bio molecules under physiological conditions. To date, most of the PEG conjugated proteins, peptides and targeting agents, available as clinical therapeutics use monofunctional PEG derivatives, which can conjugate with only one type of functional group present in the bio molecule of interest, typically an amine or carboxyl. With recent explosion in the development of multifunctionalized bio pharmaceutics, the design and synthesis of α,ω heterobifunc tional PEG derivatives has elicited phenomenal interest.[1,6,11–13] Such heterobifunctional PEG derivatives with reactive groups such as aldehyde, primary amine, mercapto and maleimide may be useful to introduce a variety of ligands and probes at the distal end of PEGylated liposomes, polymeric micelles, synthetic polymers and metal/metal oxide based colloids. Yet, to expand the scope of hetero bio conjugation through PEG linkers on diverse combinations of ligands and substrates, further improvement in the design of heterobifunctional PEG, particu larly, from the perspective of versatility and orthogonality, is crucial.

In general, a number of features such as high yield, chemo selectivity and mild reaction conditions in aqueous media stand

[a]*Centre for Pharmaceutical Nanotechnology, Department of Pharmaceutics, National Institute of Pharmaceutical Education and Research (NIPER), Sector 67, S.A.S. Nagar, Mohali 160062, India. E mail: md manasmita@yahoo.com; sanyogjain@niper.ac.in; sanyogjain@rediffmail.com; Fax: +91 172 2214692; Tel: +91 172 2292055*

[b]*Molecular Biophysics Unit, Indian Institute of Science Bangalore, Bangalore 560012, India*

† Electronic supplementary information (ESI) available. See DOI: 10.1039/c2jm34571d

indispensable for bio conjugation reactions. In view of its high aqueous tolerance, chemical orthogonality and applicability towards diverse substrates, copper(I) catalyzed 1,3 dipolar Huisgen cycloaddition between alkynes and organic azides (CuAAc) has recently received substantial attention in diverse areas of chemistry ranging from drug design to generation of functionalized polymers and solid surfaces.[14,15] The expediency and versatility of CuAAC reactions, coupled with their high yield and specificity, pave the way for quantitative introduction of various functional groups onto polymer backbones or nano particle surfaces with highly defined structures. Therefore, the combination of heterobifunctional PEGs with "click chemistry" is a promising approach for chemoselective immobilization of functional bio molecules onto a solid support, particularly nanoparticles (NPs). Although some recent reports have demonstrated the feasibility of using heterobifunctional oligo (ethylene glycol) [EG] spacers for "click" immobilization of bio molecules onto soft liposomal or hard Au nanoparticle surfaces,[16,17] application of the same for chemoselective bio functionalization of metal oxide substrates, especially magnetic nanoparticles (MNPs) or relevant metal oxide based composi tions, is still in the age of infancy. Earlier, azido terminated heterobifunctional PEG derivatives have been used for the click biofunctionalization of solid supports including polymers and nanoparticles. Nevertheless, most of these PEGs contain primary amine, carboxyl and thiol (Azide PEG NH_2, Azide PEG COOH or Azide PEG SH) as the other reactive end.[18,19] Inter estingly, as far as surface functionalization of metal oxide substrates is concerned, phosphonates and silanes provide more robust scaffolds compared to conventional carboxyl or thiol functions. Keeping this feature in mind, Kohler *et al.* developed a trifluoroethyl ester (TFEE) terminated PEG silane in which the silane anchor facilitated self assembly on the surface of iron oxide NPs while the TFEE end was conjugated to FA *via* an ethylene diamine spacer.[5,20] Yet, the instilled TFEE end group lacks chemical orthogonality and selectivity for its complemen tary function. Subsequently, the functionalization process is fraught with the possibility of nonselective cross reaction between the TFEE terminated surface and FA, containing both amine and carboxyl groups native to its structure.

In this report, we demonstrate a novel strategy for the synthesis of orthogonally bio engineered metal oxide nano particles through the design of versatile, biocompatible linkers whose structure includes the following features: (i) a robust anchor that can bind generally to a variety of metal oxide surfaces; (ii) tailored surface groups that act as spacers or branches from the metal oxide surfaces and (iii) a general method for covalent attachment of a functional perimeter to the spacers through "click chemistry". Ligands which possess the flexibility and synthetic generality of features (i) (iii) may be categorized as "universal" ligands. Such ligands or molecules allow the construction of a broad range of functionalities for the periphery of nanoparticles with high yields and synthetic facility. In an earlier report, White *et al.*[21] demonstrated the effectiveness of this "universal ligand" strategy for orthogonal functionaliza tion of maghemite (γ Fe_2O_3) nanoparticles through linkers containing phosphonic acid/carboxylic acid at one end and a clickable azide or alkyne functionality at the other end. Although this strategy contributes an effective toolbox for orthogonal engineering of metal oxide surfaces with a diverse array of functional species, the approach has been seldom exercised for the design of biofunctionalized surfaces and hitherto, limited only to small organic molecules. We sought to extend this strategy for the design of stealth and target specific nanocarriers. Keeping in mind the positive attributes of PEGylation in terms of prolonging the residence time of MNPs in blood, we designed a novel, azido terminated, polyethylene glycol (PEG) silane that could easily self assemble on metal oxide substrates through hetero condensation between the surface hydroxyl and silane head groups of the spacer and simultaneously provide multiple clickable sites for high density, chemoselective bio conjugation. As per definition, this azido PEG silane possessed all the requi site flexibility and synthetic versatility of a so called "universal ligand". Taking superparamagnetic iron oxide nanoparticles (SPIONs) as a model carrier system, we tried to demonstrate the effectiveness of azido PEG silane based ligands for orthogonal bio engineering of nanostructured metal oxides. As a proof of concept, we clicked propargyl folate (an alkyne derivative of the well known cancer targeting agent, folic acid) onto the surface of azido PEG silane immobilized magnetite (Fe_3O_4) nanoparticles (MNPs). By integrating appropriate near infrared fluorescent (NIRF) dyes (Alexa Fluor 647/680) on the surface of MNPs, we demonstrated their cancer cell specific internalization *in vitro* and biodistribution *in vivo*. The presence of an intermediate PEG spacer between the MNP core and targeting ligand not only rendered the conjugate system hydrophilic and water dispersible but also mitigated its sequestration by the organs of the mono nuclear phagocytic system (MPS) *viz.* the liver and spleen. The dual optical and magnetic properties of this newly synthesized nanoprobe could be effectively exploited to track the intracel lular localization and biodistribution of NPs through combined MR and NIRF imaging. Together, these results provided a strong motivation for future use of "clickable PEG silanes" in the chemoselective synthesis of multimodal, active targeting MNPs.

2. Materials and methods

2.1. Materials

Anhydrous ferric chloride ($FeCl_3$) and ferrous chloride tetrahy drate ($FeCl_2 \cdot 4H_2O$) were obtained from Merck, Germany. Polyethylene glycol, M.W. 570 630 (PEG 600), folic acid (FA), dicyclohexyl carbodiimide (DCC), methane sulphonyl chloride, triphenyl phosphine, propargyl amine, sodium azide (NaN_3), copper sulphate pentahydrate ($CuSO_4 \cdot 5H_2O$), sodium ascor bate, neutral red, rhodamine 1, 2, 3 and agarose were purchased from Sigma Chemical Co. (St. Louis, MO, USA). Alexa Fluor (AF) dyes for *in vitro* and *in vivo* imaging were procured from Invitrogen. Cell lines for *in vitro* experiments were obtained from the National Centre for Cell Science (NCCS), Pune. Culture media, fetal bovine serum and antibiotic antimycotic solution were procured from PAA, Austria. All solvents and reagents, unless otherwise stated, were of analytical grade. Commercially available dimethyl sulphoxide (DMSO) was dried over calcium hydride and purified *via* reduced pressure distillation. Pyridine (C_5H_5N) and triethyl amine (Et_3N) were dried over KOH and distilled prior to use. Mesityl chloride was purified *via* short path distillation.

2.2. Methods

2.2.1. Synthesis

2.2.1.1. Synthesis of α amino, ω azido PEG 600. The synthesis of the proposed PEG silane is schematized in Fig. 1. The synthesis process for the azido PEG amine was modified from previous methods for the desymmetrization of oligo ethylene glycols.[22] For the present study, PEG (M.W. 570 630) was chosen as the polymeric precursor because PEGs having an M.W. in the range of 400 600 are widely used in clinically approved, pharmaceutical formulations due to their high water solubility as well as low toxicity profile. Even from the stand point of colloidal stability or aqueous dispersibility, surface modification of any NP composition with low M.W. poly ethylene glycols results in higher monolayer packing densities and subsequently improves particle dispersion through steric stabilization.[23] In a typical procedure, methyl sulphonyl chloride (mesityl chloride, CH_3SO_2Cl) was added drop wise to a solution of PEG 600 (5 g, 8.33 mmol) in tetrahydrofuran (THF, 10 ml) under ice cold conditions and inert (N_2) atmosphere. Et_3N (12 ml, 9.1 mmol) in THF (20 ml) was added drop wise over a time period of five minutes. A yellow white precipitate was formed during this procedure and the mixture was stirred on the ice bath for another one hour. After that, the ice bath was removed and stirring was continued for an additional 3.5 h with occasional swirling of the mixture. Water (10 ml) was added to the mixture to facilitate dissolution of the solid formed in course of the reaction. A bilayer was formed inside the flask due to the immiscibility of unreacted CH_3SO_2Cl with water. The biphasic solution was cooled in a cold water bath. Sodium bicarbonate ($NaHCO_3$), followed by excess sodium azide (NaN_3), was added to the reaction mixture and stirring was continued. Sodium bicarbonate was added in order to prevent the transformation of azide into highly toxic and explosive hydrazoic acid, HN_3, under acidic conditions. THF was distilled off from the reaction mixture following a 24 h reflux of the mesylate with azide. Thereafter, the reaction mixture was partitioned in diethyl ether and water. The aqueous layer was extracted 5 6 times with 50 ml aliquots of diethyl ether (Et_2O) and each Et_2O layer was back washed with the same 50 ml aliquot of brine solution. Finally, the Et_2O layers were combined, dried over sodium sulfate, filtered, and concentrated by rotary evaporation. Traces of solvent were removed by evacuation to yield 4.1 g of the diazide as a yellowish brown oil (67%). Following transformation of dimesylate into diazide, the diazide compound (4 g) was stirred with 20 ml of 0.65 M aqueous H_3PO_4 while triphenyl phosphine in diethyl ether was added drop wise to the solution for 45 minutes as suggested by Schwabacher *et al.*[22] The reaction with triphenyl phosphine under high dilution conditions facilitated a clean transformation of the bis azido intermediate into its corre sponding mono amine derivative, as long as the ether layer is in vigorously stirred contact with dilute aqueous phosphoric acid. Since diazides are readily separable by extraction from amines, we sought to carry the transformation of diazide into azido amine to low conversion, separate the monoamine immediately after its formation and recycle the unreacted diazide. The pres ence of acid in the reaction mixture facilitated the extraction of the monoamine into the aqueous layer and subsequently sequestered it from contact with ether soluble phosphine, thereby preventing over reduction. The aqueous layer was separated after 24 h stirring and extracted with diethyl ether and KOH was added to it. The mixture was cooled to 4 °C for another 16 h, followed by removal of Ph_3PO by filtration. KOH was again added to the aqueous solution, followed by 5 6 times extraction with small volumes of dichloromethane (CH_2Cl_2). The extracted solution was dried over Na_2SO_4, filtered and concen trated by rotary evaporation.

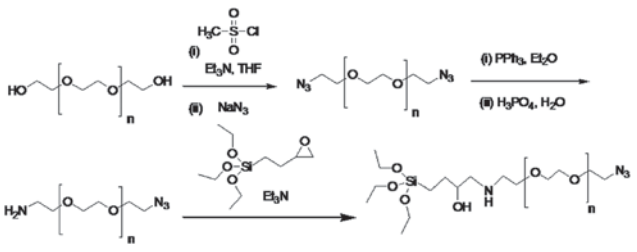

Fig. 1 A schematic representation of the synthesis of azido terminated PEG silane.

2.2.1.2. Synthesis of azido terminated PEG silane. For synthesis of azido terminated PEG silane, α amino, ω azido PEG 600 (0.1 mmol) was added to an ethanolic solution of 3 glycidoxypropyltriethoxy silane (0.09 mmol). Et_3N (0.14 mmol, 20 μl) was added to the solution and the reaction mixture was left to stirring for 12 h. Excess ethanol, Et_3N and unreacted silane were removed by rotary distillation and subsequent evac uation under reduced pressure to afford the final product as a yellowish brown oil.

2.2.1.3. Immobilization of the PEG self assembled monolayer (SAM) on magnetite nanoparticles. Bare magnetite nanoparticles (average size ~10 nm) were synthesized by alkaline coprecipita tion of Fe^{3+} and Fe^{2+} according to the protocol described in our earlier reports.[24,25] For PEG SAM immobilization, azido PEG silane (40 mg, 0.05 mmol) was dissolved in a 1 : 1 (v/v) mixture of ethanol and water. A few drops of ammonia was added to the suspension in order to maintain the pH of the reaction mixture ~8 and thereby initiate the hydrolysis of the triethoxysilane [$Si(O\ CH_2CH_3)_3$] group. With an aim to optimize the coating process with regard to reactants' concentration and time, different amounts of magnetite NPs (MNPs, 0.2 0.02 mmol) suspended in 10 ml of deionized water were added to the hydrolysis mixture. The resulting suspension was ultra sonicated for different time periods (0.5 6 h), following which the surface modified MNPs were isolated *via* magnetic concentration and subsequent washings with ethanol, water and acetone. Finally, air dried samples were used for physicochemical characterization and subsequent click bio functionalization.

2.2.1.4. Click bio functionalization of the PEG SAM. For click bio functionalization of the PEG SAM, 50 mg of azido terminated MNPs were suspended in a 1 : 1 (v/v) mixture of water and ethanol (20 ml). A few drops of Et_3N were added to the reaction mixture to adjust the pH to ~8. The number of PEG chains immobilized onto the surface of MNPs was quantified using thermogravimetric (TG) analysis. The stoichiometry of click reaction was determined on the basis of a crude assumption

that the number of available azide functions on the surface of MNPs is exactly equal to the PEG chains immobilized per unit mass of NPs. In line with that approximation, different amounts of propargyl folate (4.6 32.8 mg, 9.8 68.6 μmol), dissolved in a minimum volume of DMSO, were added to the suspension of MNPs. Copper sulphate and sodium ascorbate (10 mol% of the azide) were sequentially added to the reaction mixture and allowed to stir for different time periods (1 8 h) to optimize the number of folates immobilized per unit mass of MNPs. The "clicked" MNPs were thoroughly washed with a 40% solution of ammonia, followed by magnetic concentration and repeated washing with distilled water to completely free the NPs from Cu(II). Finally, these NPs were washed with acetone, separated *via* magnetic decantation, air dried and used for subsequent characterization and *in vitro* biological studies.

2.2.1.5. Synthesis of FA MNPs without PEG linker. Bare magnetite NPs were functionalized with 3 azido propyl trie thoxysilane (AzPTES) following the same procedure, adopted for the immobilization of azido PEG silane on MNPs. Azido terminated MNPs were reacted with propargyl folate using the same procedure described in Section 2.2.1.4.

2.2.1.6. Nanoprobe synthesis for optical imaging in vitro. For *in vitro* cellular imaging, MNPs were labeled with Alexa Fluor 647 (AF 647), a structural analog of the near infrared fluorescent dye Cy5.5. As a preliminary step to the preparation of fluores cent labeled NPs, a mixed SAM was formed onto the surface of MNPs by ultrasonically suspending MNPs in an ethanolic mixture of azido PEG silane and 3 aminopropyl triethoxysilane (APTES), taken in the molar ratio of 10 : 1. This process led to the formation of a mixed azide amine terminated SAM onto MNPs. Following click conjugation of FA onto the azide terminated MNPs, the free amine groups on NPs were reacted with the maleimide ester of AF 647 (0.5 mg dissolved in 50 μl of DMF) in the dark for 2 h. The resultant MNPs were separated by magnetic decantation, washed thoroughly with water to remove the free dye, and resuspended in aqueous suspension for optical imaging *in vitro*. The concentration of RITC on MNPs was obtained by measuring the fluorescence intensity of an aqueous suspension of dye labeled MNPs at 647 nm. Free AF 647 was used as the reference.

2.2.1.7. Nanoprobe synthesis for optical imaging in vivo. For optical imaging *in vivo*, azido PEG MNPs (10 mg, 1.96 μmol azide) were clicked with propargyl folate (5.88 μmol) and prop argyl amine (0.5 μmol) using the same protocol described in Section 2.2.1.4. The free amine groups generated on the surface of clicked MNPs (0.034 μmol mg^{-1}) were quantified using *p* nitrobenzaldehyde. These free amine groups were reacted with C_2 maleimide ester of the NIRF dye AF 680 (1 mg dissolved in 50 μl of DMF) using the same method described in Section 2.2.1.6. For preparation of control MNPs, bare magnetite NPs (10 mg) were surface functionalized with 3 aminopropyl trie thoxysilane (APTES, 0.5 μmol) using the same protocol as described earlier. The stoichiometric ratio of bare Fe_3O_4 to APTES was purposefully maintained equal to the molar ratio of azido PEG MNPs to propargyl amine used earlier for the preparation of AF 647 labeled FA PEG MNPs. Our intention was to keep the final amine concentration in both target and control nanoconjugates almost comparable so that both the formulations can be labeled with almost similar efficiency. Of note, the free amine groups generated on the surface of APTES MNPs was 0.037 μmol mg^{-1}, which was just slightly higher than the amine density of FA PEG MNPs. These free amine groups were labeled with AF 680 using the same protocol as adopted for clicked MNPs.

2.2.2. Physicochemical characterizations. The phase analysis of the synthesized magnetite nanopowder was performed on an X'pert Pro Phillips X ray diffractometer. The size, shape and morphology of the functionalized NPs were investigated by atomic force microscopy (AFM) using a Veeco Bioscope II atomic force microscope, equipped with a Nikone eclipse TE 2000 Sr microscope configured to nanoscope software. High resolution transmission electron microscopy (JEOL 3010, Japan) was employed to characterize the microstructure of the folate clicked MNPs. The hydrodynamic (HD) size of the particle aggregates was measured by laser light scattering using a Broo khaven 90 Plus particle size analyzer. The surface charge of the nanoparticles was investigated through zeta potential measure ments (Zetasizer 4, Malvern Instruments, UK). Unless otherwise specified, both the particle size and charges of MNPs were measured by suspending NPs in deionized water at pH 7. The surface chemistry of the nanoparticles was studied using a Thermo Nicolet Nexux FTIR model 870 spectrometer. For determination of the folate concentration in the folate clicked MNPs, a standard linear fit curve of free folic acid in DMSO was created by plotting the UV absorbance at 360 nm of several known concentrations of FA. The concentration of FA in the FA conjugated particles was determined by subtracting out the background absorbance of azido terminated MNPs with a normalized amount of iron at 360 nm. The surface compositions of azide terminated MNPs and their folate clicked counterpart were obtained by analyzing the X ray Photoelectron Spectro scopic (XPS) data using an Al K_α excitation source in an ESCA 2000 Multilab apparatus (VG microtech). For a detailed structure resolved analysis of the surface bound ligands, high resolution magic angle spinning (HR MAS) nuclear magnetic resonance (NMR) experiments were pursued. Samples for HR MAS experiments were prepared by suspending 10 mg of each nanoparticle preparation in DMSO d_6 (500 μl). HRMAS NMR analysis was carried out with a 400 MHz FT NMR spectrometer (Avance 400), equipped with a 5 mm HRMAS probe. Magne torelaxometric studies were performed according to the proce dure described in our earlier reports.[26]

2.2.3. *In vitro* cellular uptake, MR imaging and intracellular trafficking analysis

2.2.3.1. Cell culture. Cell uptake studies were performed in folate receptor (FR) positive human non small cell lung adeno carcinoma (A549) lung cancer cells[27 33] and normal Neuro 2A cells, deprived of FR. According to the standard protocol, cells (1×10^4 cells per well) were grown in Dulbecco's modified Eagle's medium supplemented with 10% (v/v) fetal bovine serum 2 mM glutamine, 100 units per ml penicillin, 100 μg ml^{-1} streptomycin, 4 mmol l^{-1} glutamine at 37 °C in a 5% CO_2 and 95% air humidified atmosphere. Confluent cultures were

harvested by trypsinization, cells counted and suitably diluted to obtain 5×10^5 cells per ml. Cell suspension (200 μl) was added in 96 well tissue culture plates and incubated overnight for cell attachment.

2.2.3.2. In vitro *cellular uptake.* Nanoparticle uptake by different cell lines was preliminarily studied by magnetically activated cell sorting (MACS) and further validated through cellular MR imaging as described in our earlier reports.[24,34] Briefly, A549 and Neuro 2A cells were cultured with different NP preparations as described in Section 2.2.3.1. After 3 h of incu bation, the cells were washed to remove free MNPs and cell sorting was performed using MACS. Nanoparticle uptake in cell lines was proportional to the percentage of magnetically positive cells detected using this method. Three replicates were measured and the results were averaged with percentage error determined through calculating the standard deviation from the mean.

2.2.3.3. Interaction with macrophages in vitro. RAW 264.7 cells (1×10^4 cells per well) were incubated with 100 μg of each type of functionalized MNPs for 12 h at 37 °C in a humidified incubator. After incubation, the petriplates were washed with warm PBS and phagocytic uptake was quantified using magnetically activated cell sorting (MACS).

2.2.3.4. In vitro *cellular MR imaging.* Samples for MR phantom imaging were prepared by suspending 10^6 cells in a 50 μl low melting 1% agarose gel. Cell suspensions cultured with different MNP concentrations (0.01 0.1 mg ml^{-1}) were loaded into 1.5 ml Eppendorf tubes and allowed to solidify at 4 °C. Samples were then sealed with additional agarose to avoid arti facts due to air susceptibility. MR imaging was performed with a 0.3 T clinical MRI scanner (HITACHI, AIRIS), using a pre fabricated sample holder. A spin echo multisection pulse sequence was selected from the Hitatchi Medical System (Version 7.0) to acquire MR phantom images. Repetition time (TR) of 2100 ms and variable echo times (TE) of 95 150 ms were used. The spatial resolution parameters were set as follows: an acquisition matrix of 256 × 256, field of view of 240 × 240 mm^2, section thickness of 8 mm and 2 averages. The MR signal intensity (SI) was obtained through the in built software. T_2 values were obtained by plotting the SI of each sample over a range of TE values. T_2 relaxation times were then calculated by fitting a first order exponential decay curve to the plot. The fitting equation was expressed as $SI = Ae^{(-TE/T_2)} + B$, where SI represents the signal intensity; TE, the echo time; A, the ampli tude; and B, the offset. The relaxivity (R_2) was calculated as the inverse of T_2.

2.2.3.5. Target specificity and intracellular trafficking. In order to confirm whether the uptake of folate PEG MNPs inside their target cells is mediated through folate receptors, competi tive inhibition studies were performed. In a typical experiment, A549 cells were cultured with FA clicked MNPs for 3 h in the absence and presence of excess folate (100 μg ml^{-1}), and confocal microscopy was performed as usual. For intracellular trafficking analysis, A549 cells were exposed to 100 μg ml^{-1} of AF 647 labeled, folate clicked MNPs. After 3 h of incubation, the cells were washed to remove the free MNPs adhered on the cell surface and confocal laser scanning microscopy was per formed using a model Olympus FV 1000. Intracellular localiza tion of MNPs was studied by labeling lysosomes and mitochondria with neutral red (NR) and rhodamine 123 (Rh123), respectively, as described in our earlier report.[35]

2.2.4. *In vivo* optical imaging and organ distribution studies. The protocol for *in vivo* bio distribution studies was duly approved by the Institutional Animal Ethics Committee (IAEC). Male Swiss mice weighing 25 30 g and 5 6 weeks old were divided into two groups ($n = 3$). AF 680 labeled FA PEG MNPs and APTES MNPs were administrated by intravenous injection through tail vein. After 3 h, the animals were anesthetized using ketamine xylazine (10 mg kg^{-1}, i.p.) and whole body fluores cence measurements were performed using a photon imager (Biospace, France). To further determine the exact bio distribution, the animals were sacrificed by cervical dislocation following which various vital organs *viz.* heart, lungs, liver, spleen and kidney were isolated and observed under a photon imager for fluorescence. The results were expressed as activity (counts per min; cpm) and images were captured.

3. Results and discussion

3.1. Orthogonal biofunctionalization of MNPs

3.1.1. Functionalization of MNPs with azido-PEG-silane. The chemical structure of the synthesized azido PEG silane was preliminarily analyzed using FTIR spectroscopy and finally authenticated *via* NMR analysis (see ESI, Fig. S1 and S2† for details). Once the synthesis of azido terminated PEG silane was confirmed with FTIR and ^1H NMR spectroscopy, we immobi lized the PEG silane onto the surface of MNPs according to the scheme depicted in Fig. 2. In order to optimize the functionali zation process in terms of reactants' concentration and time, silanization was carried out with different molar ratios of magnetite to PEG silane and for different sonication times (0.5 6 h). The Si to Fe atomic percent (a.%) ratios of various iron oxide preparations, as determined through electron dispersive EDS X ray microanalysis, are depicted in Table 1. As is evident from the data, a change in the molar ratio of Fe_3O_4 to PEG silane from 4 : 1 to 1 : 1 increases the Si to Fe (a.%) ratio from 0.178 0.215; however, a further increase in the concentration of PEG silane has hardly any impact on the elemental composition of NPs. Therefore, a 1 : 1 molar ratio of magnetite and PEG silane was chosen as the optimized reactants' concentration. To

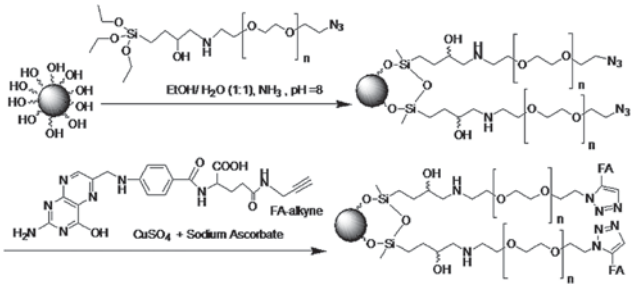

Fig. 2 Surface modification of MNPs with azido PEG silane and folate immobilization.

Table 1 Optimization of the coating process of MNPs with respect to time and reactants' concentrations

Time	0.5 h	1 h	2 h	4 h	6 h
[Fe_3O_4] : [PEG silane]	Si : Fe (a.%)				
4 : 1	0.178	0.196	0.227	0.275	0.279
2 : 1	0.198	0.215	0.244	0.286	0.287
1 : 1	0.215	0.246	0.273	0.304	0.302
1 : 2	0.216	0.248	0.279	0.336	0.341

have a rough estimation on the number of PEG chains immobilized per nanoparticle, both unmodified magnetite and its optimized PEG silane derivatized counterpart were subjected to TG analysis (see ESI, Fig. S3†). The TG thermogram of PEGylated MNPs accounted for 15.74% of the mass of stock Fe_3O_4. As determined from this weight loss, the quantity of PEG silane immobilized onto the surface of NPs was approximately 0.196 mmol g^{-1} of magnetite.

3.1.2. Click biofunctionalization of MNPs. To demonstrate the functionality of the azido terminated PEG silane, we chose to immobilize alkyne functionalized folic acid (propargyl folate) on the azido terminated silane monolayer *via* Cu(I) catalyzed azide–alkyne cycloaddition (CuAAc) reaction. Quantification of functional molecules immobilized per unit mass of the NPs was executed through UV spectrophotometry, as described in Section 2.2.6. To determine the optimum reaction time and maximum number of folates that can be conjugated per NP, both reaction time and propargyl folate concentrations were varied. Table 2 presents the amount of folate immobilized per unit mass of MNPs, when the reaction time is varied from 1–8 h and the molar ratio of polymer to folate tweaked from 1 : 1 to 1 : 7. Optimization data clearly suggest that a reaction time of 4 h and a polymer to folate ratio of 1 : 5 were suitable to achieve a high density ligand grafting on the NP surface and was taken as optimum. A prolonged reaction time or further increase in the concentration of propargyl folate had hardly any effect on the concentration of FA in the conjugated product. Under optimized conditions, approximately 0.196 mmol of azido PEG silane and 0.172 mmol of folic acid were immobilized per gram of MNPs. Since each particle contained magnetite ($d = 5.214$ g cm^{-3}) with an average radius of approximately 10 nm, the average volume and mass of Fe_3O_4 particles are 4.19×10^{-24} m^3 and 2.184×10^{-15} g respectively. Hence, 1 mg of Fe_3O_4 comprised 4.578×10^{16} particles. From these values, the average number of FA per particle was determined to be approximately 226, which was sufficiently high to execute efficient targeting *in vivo*. As is evident from our calculations, more than 85% of the surface azido groups were clicked with propargyl FA, suggesting that the transformation of surface azide groups into their corresponding triazole derivative is nearly quantitative. This high reaction yield further confirms that the majority of PEG chains immobilized onto the surface of MNPs are not at all buried within the surface and easily accessible for bio conjugation.

Table 2 Optimization of click bio functionalization with respect to time and reactants' concentration

Time	0.5 h	1 h	2 h	4 h	6 h
[PEG silane] : [propargyl folate]	Folate immobilized per unit mass of MNPs (mmol g ^{1})				
1 : 1	0.115	0.112	0.125	0.143	0.147
1 : 3	0.111	0.124	0.136	0.154	0.154
1 : 5	0.115	0.132	0.156	0.172	0.174
1 : 7	0.116	0.132	0.157	0.173	0.175

3.1.3. Surface chemistry and composition of orthogonally biofunctionalized MNPs

3.1.3.1. FTIR analysis. Unmodified MNPs exhibited a sharp band at 587 cm^{-1}, characteristic of Fe–O vibration related to the nanomagnetite core (Fig. 3). These peaks were also present in the spectra of the surface modified MNPs. Of note, PEG silane derivatized MNPs present characteristic asymmetric stretching of the azide group at around 2065 cm^{-1}, which, however, was absent in the spectra of bare MNPs. Click conjugation of propargyl folate on azide terminated MNPs was indicated by the disappearance of the 2065 cm^{-1} band and concomitant appearance of the characteristic bands of FA at 1607 cm^{-1}. A number of peaks in the range of 1500–1700 cm^{-1} were observed, which might be attributed to the various amide I (–C=O) and amide II (–NH) vibrations, characteristic of amide bonds native to the FA structure as well as those between FA and propargyl amine.

3.1.3.2. XPS analysis. Typical survey scans of azido PEG silane immobilized MNPs are presented in Fig. 4(a). The spectrum presents characteristic binding energy of Si2p, C1s, N1s, O1s and Fe2p in the range of 102–103, 284–290, 395–410, 525–535 and 710–715 eV, respectively. In addition to the survey spectrum, the high resolution N1s spectrum of these newly functionalized MNPs reveals two distinct peaks: one centered at around 400 eV and another at 406 eV, with roughly a 2 : 1 ratio of the peak integrals. The relatively lower intense, higher energy, 406 eV peak is atypical for organic nitrogen, and may be assigned to the central, electron deficient nitrogen in the azide group. Not surprisingly, reaction of this azide terminated SAM with alkyne functionalized folate reduced the 405 eV peak to the level of

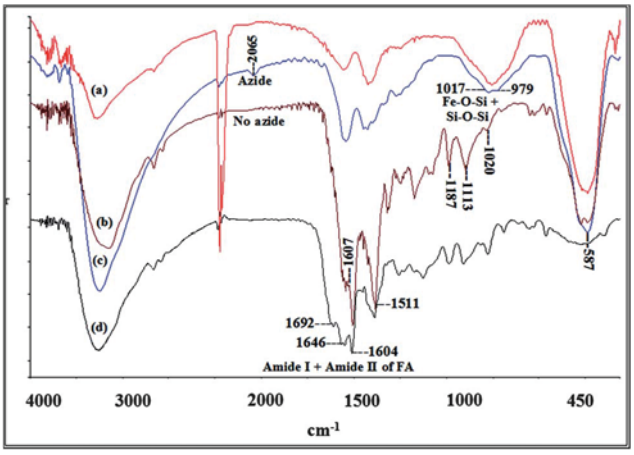

Fig. 3 FTIR spectra of (a) unmodified MNPs; (b) azido PEG silane immobilized MNPs; (c) folate "clicked" MNPs and (d) propargyl folate.

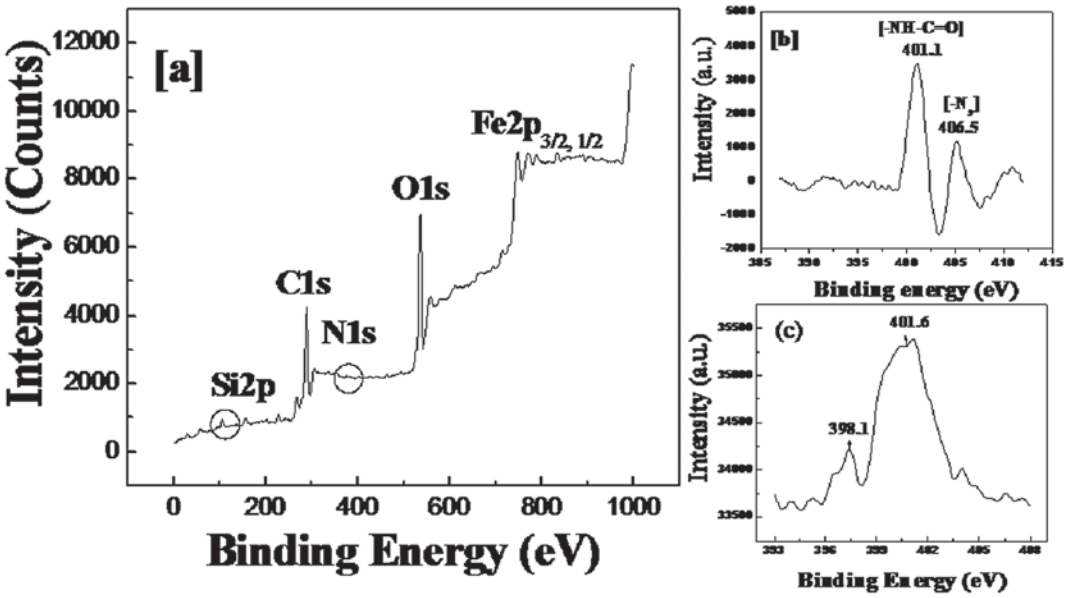

Fig. 4 XPS spectra of (a) PEG silane immobilized MNPs (survey scan); (b) high resolution N1s spectrum of azido PEG silane and (c) N1s spectrum of folate clicked MNPs.

noise. The nitrogen 1s signal at 401 eV broadened, signifying the presence of chemically distinct nitrogen atoms, corresponding to nitrogen atoms constituting the triazole ring as also the amide bonding inside the FA structure.

3.1.3.3. Fine resolved analysis of surface bound ligands: HRMAS NMR analysis. Having studied the surface chemistry and composition of functionalized MNPs *via* FTIR and XPS analysis, we attempted their fine structure resolved character ization using high resolution magic angle spinning (HRMAS NMR) spectroscopy. Fig. 5 presents the HRMAS NMR spectrum of azido terminated MNPs and their folate clicked analogue. Click immobilization of FA on the azido terminated SAM was confirmed by characteristic signals from the pteridine ring proton of FA at δ 9.8 ppm. The aromatic protons consti tuting the *p* amino benzoic acid (PABA) moiety of FA appeared in the range of δ 8.6 8.8 ppm and 7.6 7.8 ppm, which, however, were not present in the spectrum of azido MNPs. More impor tantly, a broad singlet at δ 8.1 ppm was observed, which might be assigned to the NH proton of the triazole ring. While the aromatic region is easily interpretable, definitive structural assignment in the range of δ 2.00 5.5 ppm was not possible due to the superimposition of too many proton signals in the same region. The increased complexity of this region may be attributed to the overlapping of methylene (CH_2) protons of glutamic acid moiety of FA, overlapped with the polyether (O CH_2 CH_2) bridge and terminal azido unit of PEG silane. The highly shielded proton signal in the range of δ 0.9 1.1 ppm may be assigned to methylene protons adjacent to the >Si< centre. Careful inspec tion of these ^{1}H HRMAS NMR spectra, however, revealed some interesting features, which, in general, are not perceivable in the NMR spectra of free organic molecules. As compared to the unbound PEG silane, the proton signals of MNP immobilized azido PEG silane were markedly deshielded; the extent of deshielding was even greater after click immobilization of FA. It was further interesting to note that the spectral intensity of a proton constituting the surface bound ligands was directly proportional to its distance from the NP surface. For example, the intensities of protons associated with the pteridine ring or a PABA unit of FA were disproportionally higher than that of the NH proton of the triazole ring or O CH_2 CH_2 protons of PEG silane lying in closer proximity with the MNP surface. This might be the probable reason for why the NMR spectrum of PEG silane coated MNPs presents relatively lower intense peaks that are also less sharp and well resolved, as compared to those presented by their folate clicked counterparts. The observation, however, is in close agreement with the earlier reports from our group as well as others[36] and may be attributed to (i) the con strained motion for protons closer to the MNP surface; (ii) heterogeneity due to the NP size, morphology and surface features/facets (*e.g.* terraces, edges or vertices) and (iii) spin spin relaxation (T_2) or the paramagnetic broadening effect, which critically depends on the NP size. Despite these heterogeneities, HRMAS NMR data, coupled with those of FTIR and XPS, unambiguously substantiate the orthogonal bio functionaliza tion of MNPs through this newly synthesized, azido PEG silane spacer.

3.2. Particle characteristics and stability of magnetite nanoparticles

Having confirmed the surface chemistry and composition of the functionalized MNPs, we sought to analyze their size and shape using atomic force microscopy (AFM). As is evident from Fig. 6(a), unmodified NPs of magnetite presented severe aggre gation due to magnetic anisotropy. On the other hand, AFM images of folate clicked PEGylated MNPs show distinct, spherically shaped particles with an average size of approxi mately 20 nm [Fig. 6(b)]. Although occasional aggregations are evident due to artifacts of sample preparation, overall, the coated

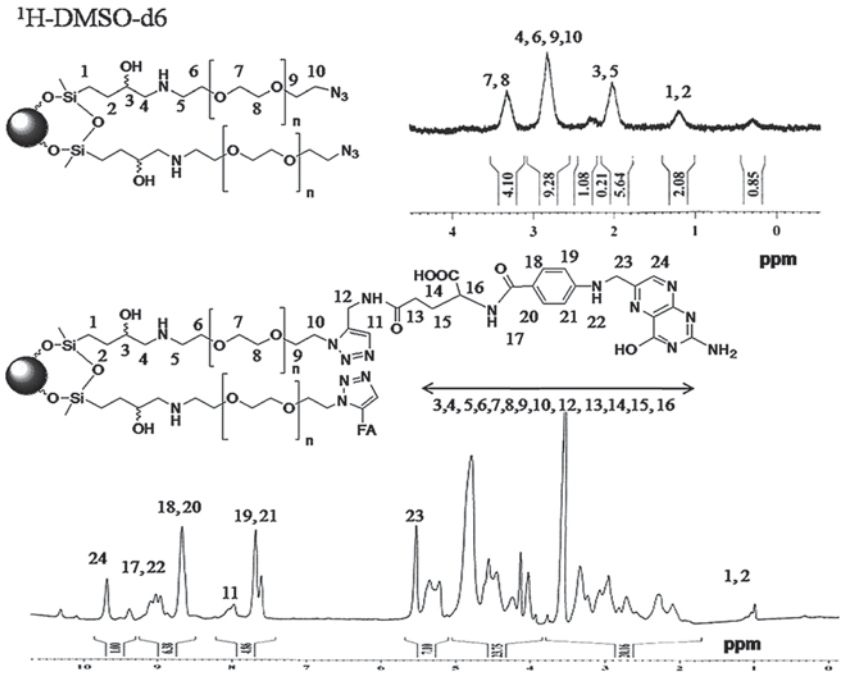

Fig. 5 [1]H HRMAS NMR spectra of azido PEG silane immobilized MNPs before and after click immobilization of alkyne functionalized folate.

MNPs presented good dispersibility in aqueous suspension. In order to revalidate the findings of AFM, HRTEM images were taken to characterize the size and dispersibility of MNPs after surface modification. Consistent with AFM observations, the HRTEM image of folate clicked MNPs show well dispersed, spherical particles with an average size ranging between 15 and 20 nm. The selected area electron diffraction (SAED) pattern (inset image) indicates the polycrystalline nature of PEG silane immobilized MNPs. The individual planes identified from the SAED pattern correlated well with those presented by the X ray

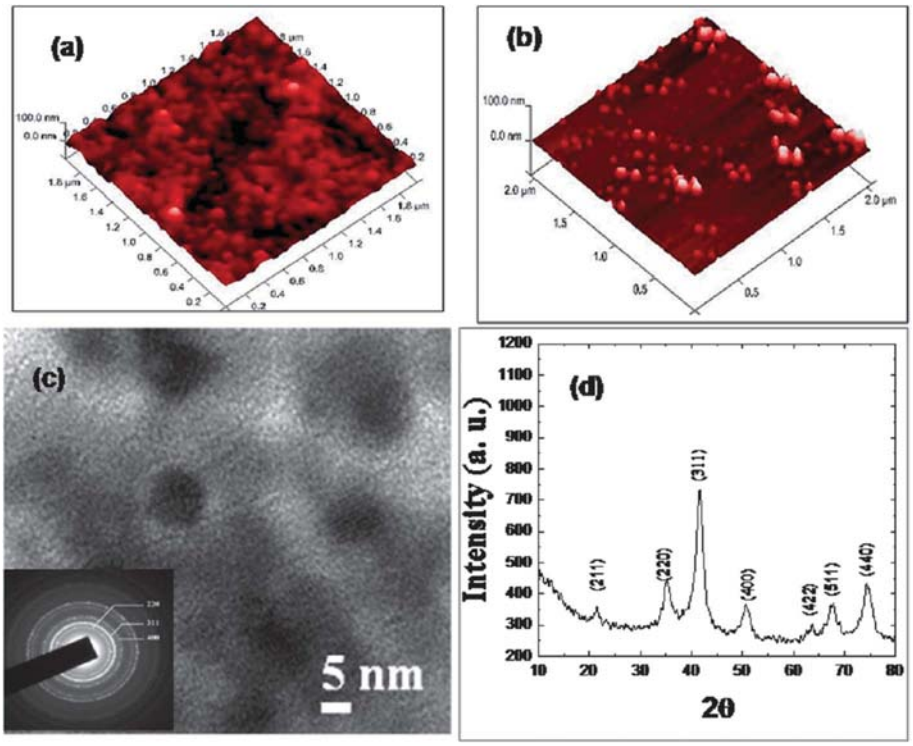

Fig. 6 (a and b) AFM images of unmodified magnetite and folate clicked magnetite NPs; (c) HRTEM image of folate clicked magnetite NPs with the SAED pattern presented as an inset; and (d) powder X ray diffractogram of folate clicked MNPs.

Table 3 Stability study of FA PEG MNPs over a period of 1 8 weeks

Time (h)	1	2	3	4	8
Size (nm)	91.2 ± 7.9	90.4 ± 8.3	96.2 ± 5.6	91.7 ± 6.9	98.2 ± 7.4
Zeta (mV)	36.3 ± 4.8	34.4 ± 4.2	35.2 ± 5.8	36.9 ± 3.9	31.4 ± 4.9
PDI	0.021 ± 003	0.021 ± 006	0.025 ± 006	0.026 ± 002	0.027 ± 004

diffractogram of PEG silane immobilized magnetite. The diffraction pattern was well consistent with that of inverse spinel magnetite [Fe_3O_4] (JCPDS card no. 85 1436); as calculated from the Debye Scherrer equation, the broadening of the peaks translated into an average core size of approximately 14.2 nm. After analyzing the size, shape and morphology of functionalized MNPs, we attempted to investigate their hydrodynamic size and zeta potential. While blank MNPs are prone to severe agglom eration (hydrodynamic size >1000 nm), an aqueous suspension of PEG self assembled MNPs presented an average size and polydispersity index (PDI) of 102 ± 6 nm and 0.289 ± 0.012 at pH 7.4. As expected, the zeta potential of azido PEG silane MNPs was near to neutral. Although no significant change in size (91.2 ± 7.9) was observed after clicking propargyl folate onto the surface of azido MNPs, a significant change in zeta potential (from 3 ± 1 mV to 36.3 ± 4.8 mV) was noted. The PDI of FA clicked MNPs was much less (0.021), suggesting that FA clicked MNPs are more uniformly dispersed as compared to their folate non conjugated PEGylated counterparts. It may be noted in this connection that the diameter of the MNPs measured by AFM or TEM is much smaller than that measured by DLS, because both AFM and TEM imaged the dry nanoparticles, whereas DLS measured the hydrated MNPs in aqueous solution. The latter included the contribution of both polymeric coatings and tar geting ligands associated with MNPs as also the hydration of PEG chains in aqueous solution.[26,37 40] As determined from DLS studies, folate clicked MNPs presented appreciable stability in aqueous medium. Their stable nature was manifested in their HD, PDI and zeta potential values, which remained unaffected for at least two months (Table 3). It may further be noted that functionalization of MNPs with PEG silane and folate had no detrimental effect on their intrinsic superparamagnetic proper ties. The absence of hysteresis, coercivity and remanence in the magnetization curve (data not shown) corroborated the super paramagnetic nature of folate clicked MNPs. Of note, the satu ration magnetization (51.3 emu g^{-1}) was lower than that of bare magnetite NPs (~91 emu g^{-1}), which, however, could be ascribed to the organic coating associated with the nanomagnetite core.

3.3. *In vitro* cellular uptake, MR imaging and intracellular trafficking analysis

3.3.1. *In vitro* cellular uptake. Having confirmed the feasi bility of orthogonal bio functionalization using the synthesized PEG silane ligand, we sought to find out whether the design of such a "universal ligand" can aid in the formation of stealth, target specific nanocarriers. In line with that objective, we tried to investigate the interaction of these folate clicked, PEGylated MNPs with: (i) a cancer cell line expressing reckonable levels of folate receptor; (ii) a normal cell line lacking measurable levels of folate receptor and (iii) a murine macrophage cell line RAW 267.4. Amongst cancer cell lines, human lung adenocarcinoma (A549) cells were chosen as our cellular target because (i) lung cancer is among the most common sites of the origin of meta static cancer through migration of lung cancer cells *via* the circulation;[41] (ii) A549 cells present a flat morphology and are therefore one of the most preferred cell lines for colocalization studies. Cell uptake was preliminarily quantified using MACS analysis. As is evident from Fig. 7, FA PEG MNPs exhibited a significantly higher uptake in FR positive A549 cells as compared to their non targeted counterparts *i.e.* azido PEG MNPs. These observations demonstrated active targeting of FA PEG MNPs through interaction between folate groups on the MNP surface and receptors of A549 cells. To further confirm the receptor specificity of the conjugate, the uptake of FA PEG MNPs in A549 cells was compared with their uptake by receptor negative Neuro 2A cell lines. In the case of A549 cells, MNP uptake was significantly higher for FA PEG MNPs when compared to their FA deprived counterparts. Conversely, the Neuro 2A uptake level of folate targeted nanoparticles was not only low but similar to those of the non targeted controls, suggesting that FA PEG MNPs are specifically targeted towards cancer cells. The low uptake of azido PEG MNPs in either cell line was consistent with an earlier report of von Maltzahn *et al.*[42] and suggested the involvement of an FR independent internalization pathway. To confirm that FR has a distinct role in the cellular internalization of FA PEG MNPs, A549 cells, pretreated with

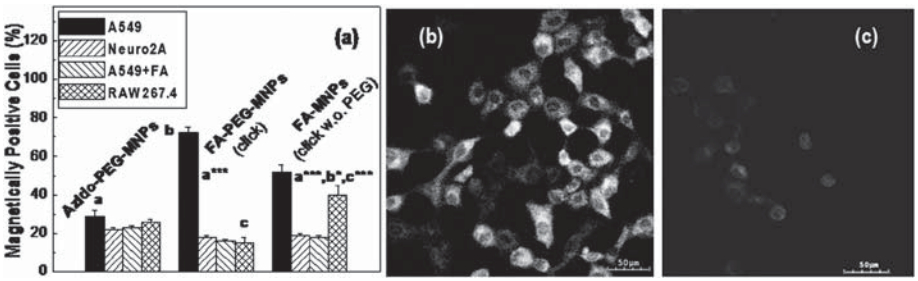

Fig. 7 (a) Uptake profile of MNPs in different cell lines quantified *via* MACS; and (b and c) confocal micrographs of A549 cells treated with FA PEG MNPs in the absence and presence of folate.

excess folate (100 μg ml^{-1}) for 1 h, were incubated with AF 647 labeled FA PEG MNPs and the uptake was visualized by confocal microscopy following a 3 h incubation. While cells without folate treatment showed a high intracellular concentration of functionalized MNPs, uptake of MNPs was nominal in the case of FA pretreated cells. A similar trend was observed when cellular uptake of MNPs was quantified by MACS. These results confirmed that free folate competes with FA present on the surface of MNPs and inhibit their interaction with FR that is already preoccupied by FA. Of note, blockage of an energy dependent pathway (with FA) had a negligible effect on the uptake of azido PEG MNPs (data not shown), corroborating the non involvement of a FR dependent endocytosis pathway. Furthermore, sodium azide pretreatment at 0 °C had no significant effect on the cell uptake of azido PEG MNPs, suggesting that endocytosis is not involved in the translocation of azido PEG MNPs to their target cells.

3.3.2. Interaction with macrophages *in vitro*. To further ensure that FA PEG MNPs are stealth enough to avoid clearance by the mononuclear phagocytic system (MPS) and reach their molecular target, the phagocytic uptake of the clicked nanoconjugate was studied *in vitro* and compared with the uptake profile of A549 cells (Fig. 7). Both azido PEG MNPs and FA PEG MNPs showed nominal uptake by macrophages, suggesting that the PEG spacer between FA and MNPs has a distinct role in evading non specific uptake of NPs by macrophages *in vitro*. To further confirm the stealth effect of the intermediary PEG spacer, the uptake of FA PEG MNPs was compared with MNPs clicked with FA *via* a non PEG based 3 azido propyl silane spacer. While uptake of FA PEG MNPs by macrophages was nominal (15 ± 3%), the percentage of magnetically labeled cells was significantly higher (40 ± 5%) in the case of MNPs conjugated to FA *via* 3 azidopropyl silane. Consequently, the uptake of FA PEG MNPs by A549 cells was also higher (72 ± 3%) when compared to their non PEGylated counterparts (52 ± 4). These results confirmed that the hydrophilic PEG backbone plays a distinct role in lowering the nonspecific phagocytosis of the clicked MNPs, which, in turn, synergized the accessibility of the targeting ligand to its cognate receptor. Our findings are also in line with earlier reports in which insertion of an oligo EG/PEG spacer between the targeting ligand and MNPs has been shown to reduce their non specific uptake by macrophages.[10,24,26,34,38,43,44] To further confirm the stealth effect of PEG, all the three MNP formulations *i.e.* azido PEG MNPs, FA PEG MNPs and FA MNPs (without PEG) were exposed to various culture media (DMEM, RPMI, *etc.*) in the presence of serum. In the case of azido PEG MNPs and FA PEG MNPs, no significant deterioration in hydrodynamic sizes was perceived even up to 96 h of incubation (Fig. S4, ESI†), indicative of a lack of protein adsorption on their surfaces. In contrast, the particle size and surface charge of FA MNPs lacking a PEG coat were significantly deteriorated within 24 h. Further, no significant alternation in the extent of cellular uptake was observed even after 24 h of incubation of FA PEG MNPs and azido PEG MNPs in 10% serum containing culture media. Of note, uptake of PEG deprived FA MNPs was significantly detrimented under similar conditions (Fig. S5, ESI†). All these observations corroborated that PEGylated MNPs, developed in course of the study, are resistant to opsonization.

3.3.3. *In vitro* MR detectibility. Although cellular uptake studies confirmed the reduced interaction of FA PEG MNPs with macrophages and their subsequent association with FR over expressing A549 cells, the results were further validated through *in vitro* cellular MR imaging studies. MR phantom samples were prepared by suspending A549 cells incubated with different concentrations of azido MNPs and folate clicked MNPs for 3 h in agarose. The T_2 weighed phantom image of cells incubated with the latter showed a significant negative contrast enhancement in comparison to its non targeted control, suggesting an effective, target specific internalization of the clicked MNPs by A549 cells [Fig. 8(a)]. At all NP concentrations, cells incubated with FA PEG MNPs presented a shorter relaxation time as compared to those treated with azido PEG MNPs. It may however be noted that at a very low concentration of MNP incubation (0.01 mg ml^{-1}), the T_2 relaxation time of azido PEG MNP incubated cells had insignificant differences with respect to control. At a higher concentration of incubation (0.05 0.1 mg ml^{-1} MNPs), some darkening in signal intensity was also observed for the non targeted control, which, however, may be attributed to the nonspecific internalization of nanometer sized particles inside their target cells. The relative relaxation times of both the preparations were quantified through T_2 weighted spin echo MR images. Fig. 8(b) shows the T_2 relaxation time as a function of particle concentration in cell culture media. A549 cells cultured with folate clicked MNPs had a shorter T_2 relaxation time (higher relaxivity) than their non targeted counterparts due to the enhanced magnetism, which, perhaps, might have resulted from elevated uptake of the former by A549 cells in comparison to the latter. To further confirm the target specificity of the synthesized conjugate, *in vitro* cellular imaging of A549 cells, Neuro 2 cells and macrophages, cultured with 0.01 0.1 mg ml^{-1} of folate clicked MNPs for 1 12 h was performed. Within 3 h of incubation, T_2 weighed MR phantom images show a significant signal darkening for A549 cells as compared to RAW macrophages and normal Neuro 2 cell lines. Among all the three cell lines, the highest T_2 relaxivity was observed for A549 cells cultured with FA PEG MNPs [Fig. 8(c) and (d)]. Furthermore, it may be noted that uptake of clicked MNPs in A549 cell lines did not show any remarkable improvement in the duration of 3 12 h, which suggests that internalization of MNPs by these cell lines reached a saturation stage within 3 h. Since darkening of signal intensity was nominal for MNP treated macrophages, even after 12 h of incubation, it may be assumed that introduction of an intermediate PEG spacer between the MNP core and the targeting ligand helped the NPs in evading non specific clearance by macrophages. All these results highlighted the usefulness of clickable PEG silanes as a universal ligand for orthogonal functionalization of metal oxide substrates with bioactive ligands and consequently aid in their transformation into a stealth, cancer targeted, MR imaging probe.

3.3.4. Intracellular trafficking and cytotoxicity of "click" nanoparticles. Intracellular trafficking of endocytosed nanoparticles involves important cell nanoparticles interaction, a thorough understanding of which is necessary to develop new

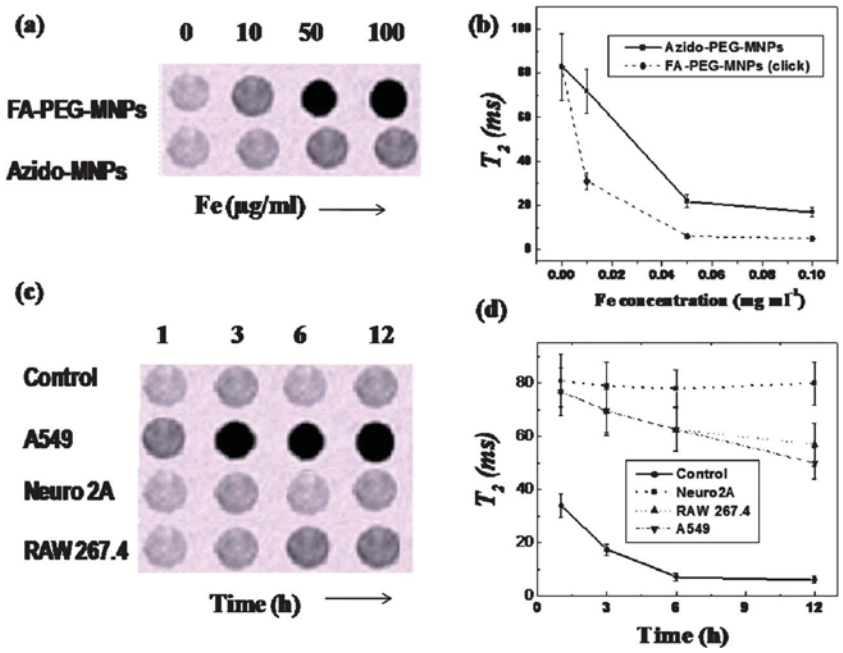

Fig. 8 (a and c) T_2 weighted spin echo MR phantom images and (b and d) relaxation analysis of cancer/normal cells incubated with 0 100 μg ml ^{1} of various MNP preparations.

molecular transporters for cancer theragnostics. To apprehend the intracellular pathway of clicked MNPs, A549 cells were incubated with FA PEG MNPs for 3 h following which their colocalization with various cell organelles (lysosome, mito chondria, *etc.*) was carefully scrutinized and compared with folate non conjugated, PEGylated MNPs (plain azido PEG MNPs). For confocal imaging studies, both MNP preparations were labeled with a NIR dye, AF 647 as described in Section 2.2.1.6. Confocal images of AF 647 labeled FA PEG MNPs and plain PEGylated MNPs are displayed in Fig. 9. The sub cellular distribution of cell internalized MNPs was tracked by staining cellular lysosomes and mitochondria with Neutral Red (NR, red fluorescence) and Rhodamine 123 (Rh123, green fluorescence) respectively. Colocalization in the entire field of view was determined through scattered plot analysis. The extent of colocalization between AF 647 labeled MNPs and an organelle specific fluorescence dye was measured in terms of Pearson's correlation coefficient (r); in general, a colocalization coefficient close to or greater than 0.5 ($r \geq 0.5$) indicated good colocaliza tion. In this context, it may be noted that the colocalization determined in the entire field of view (scatter plot) cannot precisely discriminate between fluorescence associated with MNPs adhered to the cell surface from those present intracel lularly. To confirm the colocalization profile, line plot analysis was performed to determine the variations in fluorescence intensity along a line. Yet again, the line plots measure fluores cence intensity, just in one dimension. To revalidate the quanti tative colocalization results, box plot analyses were performed which measured the changes in fluorescence intensity in two dimensions *i.e.* X and Y. Consistent with the results of MACS based cell uptake and *in vitro* cellular MR imaging, folate clicked MNPs exhibited a significantly higher uptake in comparison to their non targeted counterparts. Lower uptake of azido PEG MNPs was not unusual and is consistent with earlier literature, in which the presence of hydrophilic PEG coating on MNPs was observed to mask the interaction of NPs with target cells.[45 50] The line display of FA PEG MNPs and NR stained lysosomes is presented in Fig. 9(A) and (B). Following their cellular uptake, clicked MNPs rapidly translocated into the lysosome whereas their non targeted counterparts were mainly restricted to cellular cytoplasm. As determined from the scattered plot, the Pearson's colocalization coefficients (r) of AF 647 and NR fluorescence for azido PEG MNPs and FA PEG MNPs were determined to be 0.2 and 0.8 respectively, which indicated that the clicked MNPs show good colocalization with lysosomes. The results were further supported by line and box plot analysis [Fig. 9]. As indicated by mechanistic studies, internalization of FA PEG MNPs in A549 cells was mediated by FR. Binding of FA PEG MNPs to FR possibly leads to the formation of endocytic vesicles,[51] which possibly favored the intracellular trafficking of MNPs to lysosomes.

Line displays of AF 646 labeled MNPs and Rh123 stained mitochondria are presented in Fig. 10(a) and (b). While the Pearson coefficient for the localization of AF 647 and Rh123 was less than 0.5 in the case of azido PEG MNPs, we observed very prominent fluorescence emissions of FA PEG MNPs in the mitochondria ($r > 0.7$). The observation seems to be paradoxical because FA PEG MNPs, being negatively charged (zeta poten tial $\sim$ 36.3 ± 4.8 mV), are likely to be repelled by the negative mitochondrial membrane potential and revert back to the plasma membrane. To account for the observed colocalization profile of FA PEG MNPs, we tried to look into the different possibilities that might have facilitated the trafficking of MNPs into mito chondria. It may happen that FA PEG MNPs are initially translocated into lysosomes *via* an endosomal pathway wherein the low pH and nonspecific proteases accelerate the hydrolysis of

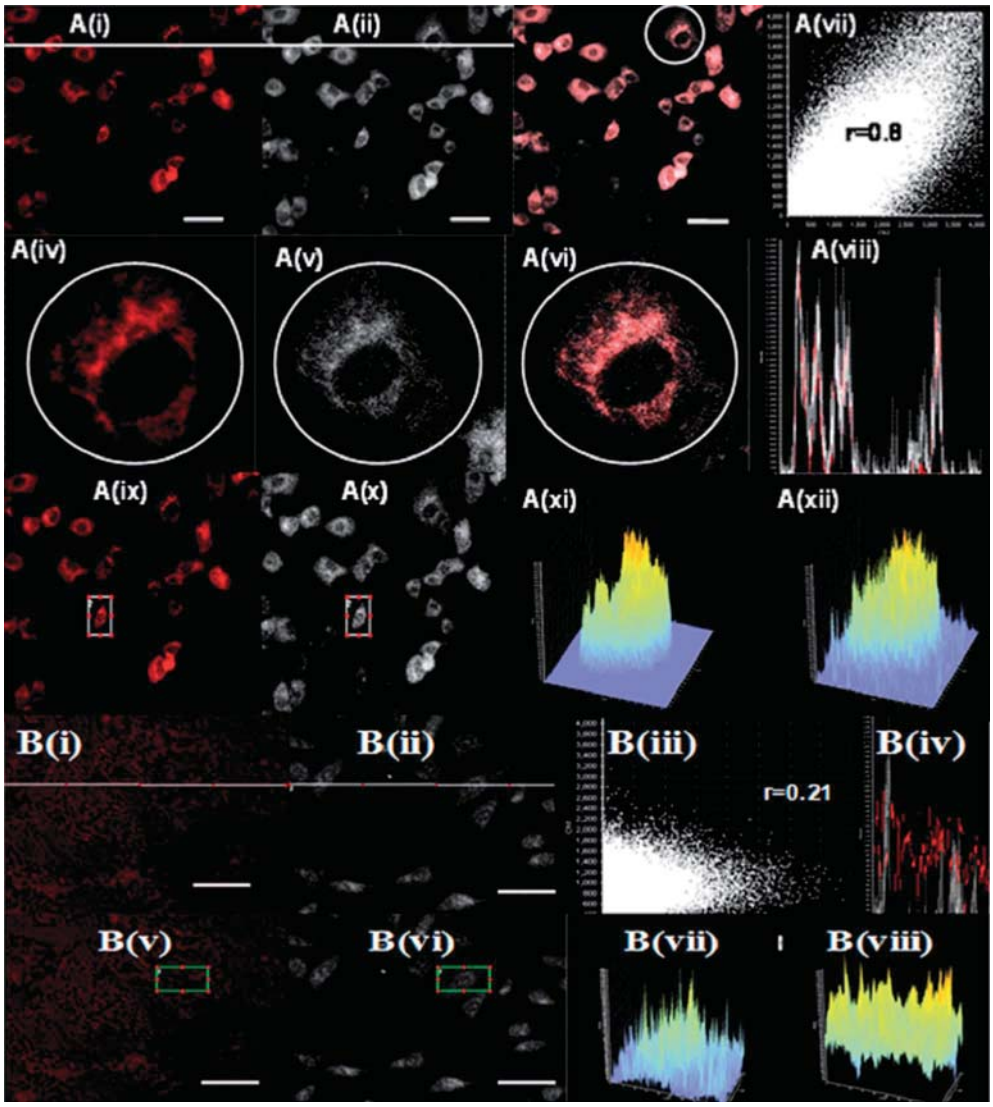

Fig. 9 Intracellular trafficking of A549 cells incubated with (A) FA PEG MNPs and (B) azido PEG MNPs; for incubation type A, (i) and (ii) represent a line display of NR and AF 647 fluorescence; (iii) overlay of AF 67 and NR fluorescence; (iv vi) enlarged view of NR stained lysosomes, AF 647 labeled CNTs and overlay of AF 647+ NR fluorescence; (vii) scattered plot; (viii) line plot; (ix and x) box display of AF 647 fluorescence and NR stained lysosomes; and (xi and xii) box plot of NR and AF 647 fluorescence. For incubation type B, (i) and (ii) represent a line display of NR and AF 647 fluorescence; (iii) scatter plot; (iv) line plot; (v and vi) box display; and (vii and viii) box plot. The white bar corresponds to 50 nm scale.

the amide bond between FA and propargyl amine[52] so that MNPs are left with some free amine groups on their surface. Cationization of MNPs may facilitate their fusion with endo somes, escape into the cytosol *via* the proton sponge effect and subsequent interaction with the negatively charged mitochon drial membrane. Charge reversal of MNPs can also occur through the protonation of a third nitrogen atom on the 1,4 disubstituted 1,2,3 triazole ring at low pH inside the lysosomes. To embark on the possibility of charge reversal inside the lyso somes, FA PEG MNPs were incubated at pH 4 for 3 h and subjected to zeta potential analysis. We found that FA PEG MNPs acquire a positive charge (9 ± 1 mV) at a low pH (data not shown) *i.e.* simulated endolysosomal conditions. Therefore, we cannot also disregard the possibility of MNP escape from the lysosomes by a mechanism similar to that operating for cationic lipids. Our hypothesis is also in line with the observations of Panyam *et al.*[53] wherein the authors showed similar charge reversal and endolysosomal escape of negatively charged PLGA nanoparticles. Apart from these possibilities, mitochondrial compartmentalization of FA PEG MNPs may be a consequence of an FR independent internalization pathway operating simul taneously along with an FR dependent pathway. As observed in our competitive inhibition studies, cellular uptake of MNPs was significantly inhibited in the presence of free FA but not completely blocked. While FR mediated endocytosis is the predominant pathway underlying the internalization of MNPs inside their cellular target, 20 25% of the internalized MNPs can also enter the cells *via* non specific mechanisms, localize in cytoplasm and carried over to mitochondria *via* a carrier medi ated uptake mechanism. To further ensure that observation of MNPs in the mitochondria is not due to dissociation of dye from the particles, the stability of dye conjugated FA PEG MNPs

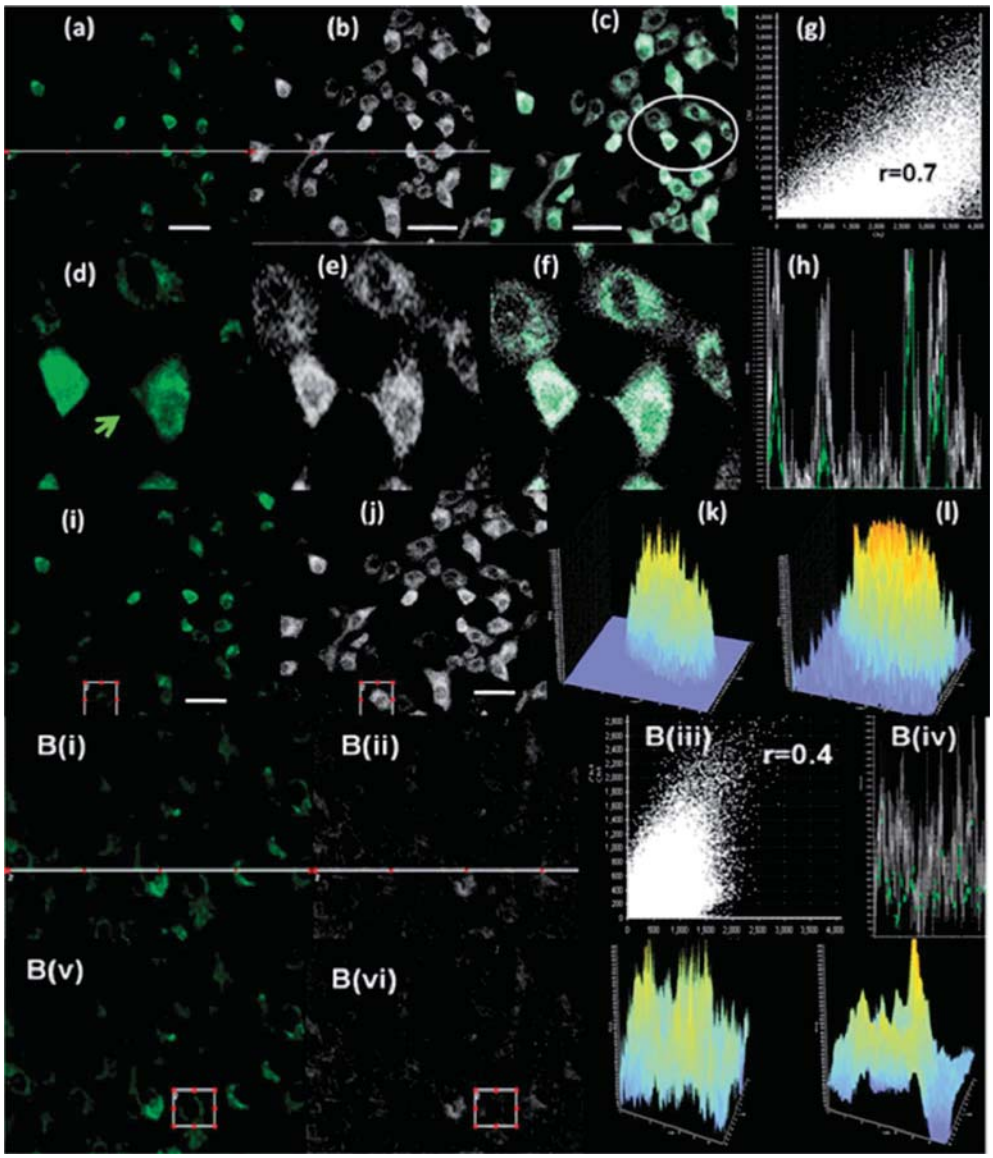

Fig. 10 Intracellular trafficking of A549 cells incubated with (A) FA PEG MNPs and (B) azido PEG MNPs; for incubation type A, (i) and (ii) represent a line display of Rh123 and AF 647 fluorescence; (iii) overlay of AF 67 and Rh123 fluorescence; (iv vi) enlarged view of Rh123 stained mitochondria, AF 647 labeled CNTs and overlay of AF 647+ Rh123 fluorescence; (vii) scattered plot; (viii) line plot; (ix and x) box display of AF 647 fluorescence and Rh123 stained mitochondria; and (xi and xii) box plot of Rh123 and AF 647 fluorescence. For incubation type B, (i) and (ii) represent a line display of Rh123 and AF 647 fluorescence; (iii) scatter plot; (iv) line plot; (v and vi) box display; and (vii and viii) box plot of Rh123 and AF 647 fluorescence. The white bar corresponds to 50 nm scale.

was evaluated in A549 cell lysate as well as simulated lysosomal conditions (*i.e.* in the presence of low pH and pancreatin). However, we did not observe any fluorescence signal of the dye either in cell extract or simulated lysosomal conditions (data not shown) even after 24 h of incubation. These observations sug gested that the observed fluorescence in mitochondria was not due to free dye but MNPs. In this regard it may be further noted that AF dyes possess negatively charged sulphonate groups and are likely to be deterred by the negatively charged mitochondrial membrane. Even though the present study is not able to conclusively determine the exact mechanism responsible for concomitant localization of FA PEG MNPs in both lysosomes and mitochondria, from cell uptake, MR imaging and colocalization studies, it is confirmed that FA MNPs enter the cells through FR receptor mediated endocytosis and localize in cytoplasm, mostly in thecal organelles like lysosomes and mito chondria. Regarding mitochondrial localization of MNPs, we should also keep in mind some important technical issues. As is evident from the confocal micrographs, Rh123 exhibits green emission whereas NR shows red emission. Because of the shorter wavelength of green emission, the emitted fluorescence is some what scattered or diffused, which might have increased the apparent colocalization to some extent.

To further ensure that clicked MNPs are noncytotoxic to cells, *in vitro* cytotoxicity studies were conducted using the conven tional MTT assay. For this purpose, A549 cells were treated with

0.001 1 mg ml^{-1} of both azido PEG MNPs and FA PEG MNPs for 24 h. In either case, no reduction in cellular viability was observed even up to 500 μg ml^{-1} of MNPs (see ESI, Fig. S6†). In either case, the IC 50 values were greater than 4 mg ml^{-1} of functionalized MNPs, which was approximately 8 times higher than the highest concentration, used for *in vitro* experi ments. These data also confirm that colocalization of "clicked" MNPs with lysosomes and mitochondria is not associated with destabilization of the lysosomal compartment or dissipation of the mitochondrial membrane potential. Cumulatively, our find ings indicate that clicked MNPs, developed in course of the study, are safe in therapeutic doses and may be potentially explored further for organelle specific delivery of lysosomal or mitochondrial targeted anticancer drugs.

3.3.5. ***In vivo* optical imaging and bio-distribution studies.** In the present study, we undertook an optical imaging based approach to track the biodistribution of our newly synthesized nanoprobe *in vivo*. As a preliminary step towards *in vivo* imaging and organ distribution studies, the terminal azido groups on PEGylated MNPs were coconjugated with alkyne folate and propargyl amine using azide alkyne click chemistry. The free amine groups on the PEG SAM were covalently conjugated with a NIRF dye (C_2 maleimide ester of AF 680) using the procedure described in Section 2.2.1.7. To analyze the stability of these magnetofluorescent NPs within the biological system, MNPs were exposed to PBS (at physiological pH) and serum for more than 72 h. MNPs were found to be stable with no visible sign of aggregation or loss of functionality (data not shown). No changes in the fluorescence signal of dye conjugated MNPs were observed even after 72 h of incubation in PBS or serum, sug gesting that the bimodal probe developed in course of the study is stable under physiological conditions. Having confirmed the stability of the dye, we sought to determine whether the azido PEG silane spacer interlinking MNPs and PEG can prevent the sequestration of NPs by liver and spleen. The *in vivo* imaging and biodistribution studies were performed in Swiss mice and employed a photon imager dedicated to noninvasive imaging of small animals. The animals were imaged prior to administration of MNPs in order to determine the value of autofluorescence background. Following this, mice were intravenously adminis tered with FA PEG MNPs and APTES MNPs devoid of a PEG linker at doses of 10 mg kg^{-1} body weight. It has been demon strated that RES uptake is the highest during the first 3 h of administration and over two thirds of the NPs are distributed into various body compartments.[54] It was however difficult to quantify the exact biodistribution of dye labeled MNPs from the intact animal images (see ESI, Fig. S7†) because the photon image represents a 2D image in which it was difficult to distin guish specific organs. All vital organs, being on the same plane,

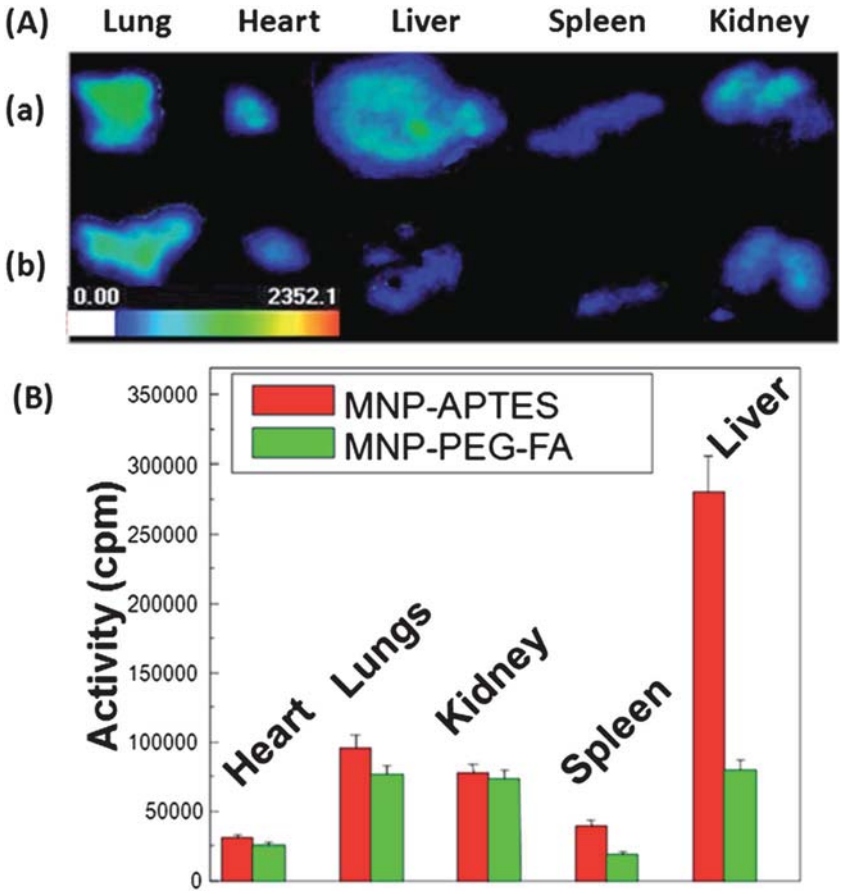

Fig. 11 (A) *Ex vivo* NIRF images of mice treated with (a) APTES MNPs (w.o. PEG linker) and (b) FA PEG MNPs; and (B) quantification of fluorescence intensity of various vital organs in mice using a photon imager.

overlapped and could not be discriminated. We, therefore, sacrificed the animals and proceeded for *ex vivo* whole organ imaging in which fluorescence intensities of all major organs (*viz.* heart, lungs, liver, spleen and kidney) were quantified. Fig. 11A(a and b) present the *ex vivo* photon images of isolated organs of a mouse treated with PEG deprived APTES MNPs and FA PEG MNPs respectively. In either case functionalized MNPs show accumulation in all major organs including the liver and spleen. While the differences in NIRF signal intensity between non MPS organs (heart, lungs, *etc.*) are insignificant, it was interesting to observe that fluorescence signal intensities of FA PEG MNPs in the liver and spleen are considerably lower than that of PEG deprived APTES MNPs. Quantitative data suggested almost four times higher accumulation of APTES MNPs in the liver as compared to its FA PEG MNPs [Fig. 11(B)]. These results unambiguously suggest that the clickable PEG silane developed in course of our study can effectively reduce sequestration of NPs by the MPS organs. Although pharmacokinetics and tumor targeting behavior of this newly synthesized nanoprobe *in vivo* is yet to be investigated, the results in hand provide a strong motivation for the future use of these clickable PEG silanes as an essential building block of stealth, target specific nanocarriers.

4. Conclusion

In conclusion, we have developed a novel, azido terminated PEG silane that can easily self assemble on a metal oxide surface through the silane anchor and simultaneously facilitate orthogonal bio functionalization of the substrate through click chemistry. This linker molecule possessed all the qualities and synthetic generality of a "universal ligand" and was effectively exploited for the chemoselective synthesis of stealth and target specific magnetofluorescent nanohybrids. The feasibility of orthogonal bio functionalization through a "universal ligand" strategy was established by covalent immobilization of azido terminated PEG silane onto the surface of magnetite NPs and their further modification with alkyne functionalized folate through CuAAc reaction. PEG SAM formation and subsequent FA immobilization were confirmed using a plethora of complementary techniques including FTIR, XPS and HRMAS NMR analyses. By further integrating a NIR dye, AF 647 with MNPs, we established that folate clicked PEGylated MNPs enter their target cells through FR mediated endocytosis and intracellularly traffic to the lysosomes and mitochondria. While the silane anchor rendered stability to the MNPs in colloidal suspension, the presence of a PEG spacer between the MNP core and the targeting ligand endowed the NPs with stealth characteristics while increasing their accessibility to the receptor site. In addition, the dual optical and magnetic properties of clicked MNPs aided in tracking their whereabouts through combined MR and optical imaging. All these results justify the effectiveness of our surface design and confirm that orthogonal functionalization of MNPs *via* a "universal ligand" strategy had no detrimental influence on the physicochemical and biological activity of the carrier as well as functional molecules tethered onto the surface of nanocarriers. In the current scientific panorama, in which the emergence of smart, multimodal NPs seems to be one of the major breakthroughs in cancer theragnostics, the development of this heterobifunctional, silane headed clickable spacer contributes a new tool box to the orthogonal bio functionalization of inorganic nanoparticles using azide alkyne click chemistry. Since functionalization of MNPs was carried out with aqueous based solvents and environment friendly reagents under benign conditions, it also constituted a novel toolbox for executing the orthogonal biofunctionalization of metal oxide based and relevant nanosystems under "green" conditions. Impressively, functionalized MNPs developed in course of the study proved their ability to accumulate in the cellular lysosomes and mitochondria, which, in future, might be explored for the development of organelle specific therapeutics based on NPs. Also, reduced accumulation of FA PEG MNPs in the liver and spleen as compared to their non PEGylated counterparts suggested the effectiveness of this newly synthesized spacer as an essential building block of long circulating nanocarriers. Finally, the positive attributes of *in vitro* and *in vivo* biodistribution studies make these newly synthesized folate clicked MNPs a prospective platform for further *in vivo* investigations.

Acknowledgements

The authors gratefully acknowledge the Department of Science and Technology (DST, New Delhi) and the Council of Scientific and Industrial Research (CSIR), Govt. of India for providing financial support for this work. The Director of NIPER is acknowledged for providing necessary infrastructural facilities. We thank Dr K.R. Patil, National Chemical Laboratory (NCL) Pune, Central Research Facility (CRF), IIT Kharagpur and SAIF, Central Drug Research Institute (CDRI, Lucknow) for assistance with XPS, HRTEM and HRMAS NMR analyses. Prof. T. K. Maiti and Mr Debasish Mishra, Department of Biotechnology, IIT Kharagpur are duly acknowledged for their useful discussions and support on MACS and *in vitro* cellular MR imaging studies. Mr Nirjhar Samanta, Midnapore Diagnostic Pvt. Ltd., Kolkata is duly acknowledged for his excellent assistance with MRI studies.

References

1 J. M. Harris and R. B. Chess, *Nat. Rev. Drug Discovery*, 2003, **2**, 214–221.
2 F. M. Veronese and G. Pasut, *Drug Discovery Today*, 2005, **10**, 1451–1458.
3 F. M. Veronese, *Biomaterials*, 2001, **22**, 405–417.
4 Y. Yamamoto, Y. Tsutsumi, Y. Yoshioka, T. Nishibata, K. Kobayashi, T. Okamoto, Y. Mukai, T. Shimizu, S. Nakagawa and S. Nagata, *Nat. Biotechnol.*, 2003, **21**, 546–552.
5 N. Kohler, C. Sun, A. Fichtenholtz, J. Gunn, C. Fang and M. Zhang, *Small*, 2006, **2**, 785–792.
6 M. J. Roberts, M. D. Bentley and J. M. Harris, *Adv. Drug Delivery Rev.*, 2002, **54**, 459–476.
7 L. Zheng, C. Peng, Q. Chen, M. Shen, R. Guo, H. Wang, X. Cao, G. Zhang and X. Shi, *Biomaterials*, 2012, **33**, 1107–1119.
8 C. Kojima, Y. Umeda, M. Ogawa, A. Harada, Y. Magata and K. Kono, *Nanotechnology*, 2010, **21**, 245104.
9 S. H. Kim, E. M. Kim, C. M. Lee, D. W. Kim, S. T. Lim, M. H. Sohn and H. J. Jeong, *J. Nanomater.*, 2012, DOI: 10.1155/2012/504026.
10 C. Sun, R. Sze and M. Zhang, *J. Biomed. Mater. Res., Part A*, 2006, **78**, 550–557.
11 S. Hiki and K. Kataoka, *Bioconjugate Chem.*, 2007, **18**, 2191–2196.
12 H. Otsuka, Y. Nagasaki and K. Kataoka, *Adv. Drug Delivery Rev.*, 2003, **55**, 403–419.
13 F. Zeng and C. Allen, *Macromolecules*, 2006, **39**, 6391–6398.
14 R. A. Evans, *Aust. J. Chem.*, 2007, **60**, 384–395.

15 J. F. Lutz and Z. Zarafshani, *Adv. Drug Delivery Rev.*, 2008, **60**, 958 970.
16 L. Nebhani and C. Barner Kowollik, *Adv. Mater.*, 2009, **21**, 3442 3468.
17 A. Von Knethen and B. Brune, *FASEB J.*, 1997, **11**, 887.
18 S. Hiki and K. Kataoka, *Bioconjugate Chem.*, 2007, **18**, 2191 2196.
19 G. von Maltzahn, Y. Ren, J. H. Park, D. H. Min, V. R. Kotamraju, J. Jayakumar, V. Fogal, M. J. Sailor, E. Ruoslahti and S. N. Bhatia, *Bioconjugate Chem.*, 2008, **19**, 1570 1578.
20 N. Kohler, G. E. Fryxell and M. Zhang, *J. Am. Chem. Soc.*, 2004, **126**, 7206 7211.
21 M. A. White, J. A. Johnson, J. T. Koberstein and N. J. Turro, *J. Am. Chem. Soc.*, 2006, **128**, 11356 11357.
22 A. W. Schwabacher, J. W. Lane, M. W. Schiesher, K. M. Leigh and C. W. Johnson, *J. Org. Chem.*, 1998, **63**, 1727 1729.
23 M. D. Butterworth, L. Illum and S. S. Davis, *Colloids Surf., A*, 2001, **179**, 93 102.
24 M. Das, D. Mishra, T. K. Maiti, A. Basak and P. Pramanik, *Nanotechnology*, 2008, **19**, 415101.
25 M. Das, D. Bandyopadhyay, D. Mishra, S. Datir, P. Dhak, S. Jain, T. K. Maiti, A. Basak and P. Pramanik, *Bioconjugate Chem.*, 2011, **22**, 1181 1193.
26 M. Das, D. Mishra, P. Dhak, S. Gupta, T. K. Maiti, A. Basak and P. Pramanik, *Small*, 2009, **5**, 2883 2893.
27 S. Santra, C. Kaittanis, J. Grimm and J. M. Perez, *Small*, 2009, **5**, 1862 1868.
28 A. Asati, S. Santra, C. Kaittanis, S. Nath and J. M. Perez, *Angew. Chem., Int. Ed.*, 2009, **48**, 2308 2312.
29 S. Santra, C. Kaittanis and J. M. Perez, *Mol. Pharm.*, 2010, **7**, 1209 1222.
30 S. Santra, C. Kaittanis, O. J. Santiesteban and J. M. Perez, *J. Am. Chem. Soc.*, 2011, **113**(41), 16680 16688.
31 S. Santra and J. M. Perez, *Biomacromolecules*, 2011, **12**(11), 3917 3927.
32 C. Kaittanis, S. Santra, O. J. Santiesteban, T. J. Henderson and J. M. Perez, *J. Am. Chem. Soc.*, 2011, **133**(10), 3668 3676.
33 C. Kaittanis, S. Santra and J. M. Perez, *J. Am. Chem. Soc.*, 2009, **131**, 12780 12791.
34 M. Das, P. Dhak, S. Gupta, D. Mishra, T. K. Maiti, A. Basak and P. Pramanik, *Nanotechnology*, 2010, **21**, 125103.
35 N. K. Swarnakar, A. K. Jain, R. P. Singh, C. Godugu, M. Das and S. Jain, *Biomaterials*, 2011, **32**, 6860 6874.
36 L. Polito, M. Colombo, D. Monti, S. Melato, E. Caneva and D. Prosperi, *J. Am. Chem. Soc.*, 2008, **130**, 12712 12724.
37 O. Veiseh, C. Sun, C. Fang, N. Bhattarai, J. Gunn, F. Kievit, K. Du, B. Pullar, D. Lee and R. G. Ellenbogen, *Cancer Res.*, 2009, **69**, 6200.
38 F. Sonvico, S. Mornet, S. Vasseur, C. Dubernet, D. Jaillard, J. Degrouard, J. Hoebeke, E. Duguet, P. Colombo and P. Couvreur, *Bioconjugate Chem.*, 2005, **16**, 1181 1188.
39 M. Das, D. Mishra, T. Maiti, A. Basak and P. Pramanik, *Nanotechnology*, 2008, **19**, 415101.
40 M. Das, P. Dhak, S. Gupta, D. Mishra, T. K. Maiti, A. Basak and P. Pramanik, *Nanotechnology*, 2010, **21**, 125103.
41 C. Alix Panabières, S. Riethdorf and K. Pantel, *Clin. Cancer Res.*, 2008, **14**, 5013 5021.
42 G. von Maltzahn, Y. Ren, J. H. Park, D. H. Min, V. R. Kotamraju, J. Jayakumar, V. Fogal, M. J. Sailor, E. Ruoslahti and S. N. Bhatia, *Bioconjugate Chem.*, 2008, **19**, 1570 1578.
43 H. Lee, E. Lee, K. Do Kyung, N. K. Jang, Y. Y. Jeong and S. Jon, *J. Am. Chem. Soc.*, 2006, **128**, 7383 7389.
44 Y. Zhang, N. Kohler and M. Zhang, *Biomaterials*, 2002, **23**, 1553 1561.
45 S. Mishra, P. Webster and M. E. Davis, *Eur. J. Cell Biol.*, 2004, **83**, 97 111.
46 E. C. Gryparis, M. Hatziapostolou, E. Papadimitriou and K. Avgoustakis, *Eur. J. Pharm. Biopharm.*, 2007, **67**, 1 8.
47 B. Romberg, W. E. Hennink and G. Storm, *Pharm. Res.*, 2008, **25**, 55 71.
48 R. L. Hong, C. J. Huang, Y. L. Tseng, V. F. Pang, S. T. Chen, J. J. Liu and F. H. Chang, *Clin. Cancer Res.*, 1999, **5**, 3645 3652.
49 T. Kaasgaard, O. G. Mouritsen and K. Jorgensen, *Int. J. Pharm.*, 2001, **214**, 63 65.
50 H. Hatakeyama, H. Akita, K. Kogure, M. Oishi, Y. Nagasaki, Y. Kihira, M. Ueno, H. Kobayashi, H. Kikuchi and H. Harashima, *Gene Ther.*, 2006, **14**, 68 77.
51 M. S. Pandey, E. N. Harris, J. A. Weigel and P. H. Weigel, *J. Biol. Chem.*, 2008, **283**, 21453.
52 N. Kohler, C. Sun, J. Wang and M. Zhang, *Langmuir*, 2005, **21**, 8858 8864.
53 J. Panyam, W. E. N. Z. Zhou, S. Prabha, S. K. Sahoo and V. Labhasetwar, *FASEB J.*, 2002, **16**, 1217 1226.
54 C. Goncalves, E. Torrado, T. Martins, P. Pereira, J. Pedrosa and M. Gama, *Colloids Surf., B*, 2010, **75**, 483 489.

